

Inferring past effective population size from distributions of coalescent times

Lucie Gattepaille^{*,1}, Torsten Günther^{*} and Mattias Jakobsson^{*,1,†}

^{*}Department of Organismal Biology, Uppsala University, Uppsala, Sweden, [†]Science for Life Laboratory, Uppsala University, Uppsala, Sweden

ABSTRACT Inferring and understanding changes in effective population size over time is a major challenge for population genetics. Here we investigate some theoretical properties of random mating populations with varying size over time. In particular, we present an exact solution to compute the population size as a function of time, $N_e(t)$, based on distributions of coalescent times of samples of any size. This result reduces the problem of population size inference to a problem of estimating coalescent time distributions. To illustrate the analytic results, we design a heuristic methods using a tree-inference algorithm and investigate simulated and empirical population-genetic data. We investigate the effects of a range of conditions associated with empirical data, for instance number of loci, sample size, mutation rate, and cryptic recombination. We show that our approach performs well with genomic data ($\geq 10,000$ loci) and that increasing the sample size from 2 to 10 greatly improves the inference of $N_e(t)$ whereas further increase in sample size results in modest improvements, even under a scenario of exponential growth. We also investigate the impact of recombination and characterize the potential biases in inference of $N_e(t)$. The approach can handle large sample sizes and the computations are fast. We apply our method to human genomes from four populations and reconstruct population size profiles that are coherent with previous finds, including the Out-of-Africa bottleneck. Additionally, we uncover a potential difference in population size between African and non-African populations as early as 400 thousand years ago. In summary, we provide an analytic relationship between distributions of coalescent times and $N_e(t)$, which can be incorporated into powerful approaches for inferring past population sizes from population-genomic data.

KEYWORDS Effective population size; coalescent time; Human evolution;

Natural populations vary in size over time, sometimes drastically, like the bottleneck caused by the domestication of the dog (Lindblad-Toh *et al.* 2005) or the explosive growth of human populations in the past 2000 years (Cohen 1995). Inferring population size as a function of time has many applications, for instance, better understanding of major ecological or historical events' impact on humans such as glacial periods (Lahr and Foley 2001; Palkopoulou *et al.* 2013), agricultural shifts or technological advances (Boserup 1981), and colonization of new areas (Ramachandran *et al.* 2005; Jakobsson *et al.* 2008). Knowledge about the demographic history is also important for studies of natural selection in order to avoid

spurious finds (Li *et al.* 2012; Nielsen 2005).

Estimating past effective population size has gained considerable interest in recent years, in particular with the development of methods such as the Bayesian skyline plots implemented in BEAST (Drummond *et al.* 2012); see Ho and Shapiro (2011) for a review of this school of methods. More recently, methods based on the sequentially Markovian coalescent (SMC and its refined version SMC', McVean and Cardin 2005; Marjoram and Wall 2006), such as PSMC (Li and Durbin 2011), MSMC (Schiffels and Durbin 2013), DiCal (Sheehan *et al.* 2013) and Bayesian approaches (Palacios *et al.* 2015) have advanced our ability to infer past population sizes. The former type of methods can use relatively large sample sizes, but can only handle modest numbers of loci, and these methods have often been used for analyzing mitochondrial DNA. The latter group of methods can handle genome-wide data and explicitly model

Copyright © 2016 by the Genetics Society of America
doi: 10.1534/genetics.XXX.XXXXXX

Manuscript compiled: Thursday 15th September, 2016%

[†]Department of Organismal Biology, Uppsala University, Norbyvägen 18C, 75 236 Uppsala, Sweden. lucie.gattepaille@ebc.uu.se, mattias.jakobsson@ebc.uu.se

recombination using a Markovian assumption for neighboring gene-genealogies (McVean and Cardin 2005). PSMC works with a single (diploid) individual, which leads to simple underlying tree topologies without requiring phase information. However, the inference power is limited, in particular in the recent past, as most coalescences in a sample of size 2 are not expected to occur in that period (Li and Durbin 2011). MSMC and DiCal extend this approach by using information from multiple samples. MSMC focuses on the first coalescence event in the sample at each locus and ignores the remaining coalescence events. The algorithm can deal with genome-wide data in a computationally efficient way. DiCal, on the other hand, uses all coalescent events in the gene-genealogies to provide estimates of the population size, assuming a Markov property between sites as well (Sheehan *et al.* 2013). The algorithm quickly becomes computationally intensive as the sample size increases and analyzing genome-wide data is challenging. Palacios *et al.* (2015) develop an interesting Bayesian non-parametric approach building on the SMC' model and assuming known gene genealogies, which shows promising accuracy for inferring relatively simple past population sizes using moderate number of loci.

There are two important steps for most of these types of approaches: the inference of the underlying gene-genealogies, and the inference of population size as a function of time from the inferred genealogies. In this paper we introduce the **Population Size Coalescent-times based Estimator** (Popsicle), an analytic method for solving the second part of the problem. We derive the relationship between the population size as a function of time, $N_e(t)$, and the coalescent time-distributions by inverting the relationship of the coalescent time-distributions and population size that was derived by Polanski and colleagues (Polanski *et al.* 2003), where they expressed the distribution of coalescent times as linear combinations of a family of functions that we describe below. The theoretical correspondence between the distributions of coalescent times and the population size over time implies a reduction of the full inference problem of population size from sequence data to an inference problem of inferring gene-genealogies from sequence data. This result represent a theoretical advancement that can dramatically simplify the computation of $N_e(t)$ for many existing and future approaches to infer past population sizes from empirical population-genetic data.

In this article, we first present the core theoretical result; the exact correspondence between the set of distributions of coalescent times for samples of any size and the population size as a function of time. We then provide an illustration of the performance of the theoretical result on simulated gene-genealogies, including several assessments of how different factors (number of loci, sample size, presence of recombination) can affect the performance of our approach. Finally, we illustrate how our theoretical result could be used to estimate population size over time from sequence data (simulated and experimental). Since this latter part necessitate a method to infer gene-genealogies from sequence data, we provide a simple algorithm to perform this particular task, based on the UPGMA algorithm and properties of the mutation process for the coalescent (the technical details are described in the Methods section).

Model and Methods

Distributions of coalescent times and $N(t)$

Under the constant population size model, the waiting times T_n, T_{n-1}, \dots, T_2 between coalescent events are independent exponentially distributed random variables. In particular, the time T_k during which there are exactly k lineages follows an exponential distribution with rate $\binom{k}{2}/N$ generations. When population size varies as a function of time ($N = N(t)$), the waiting times to coalescence are no longer independent of each other. Specifically, for $k \in [2, n-1]$, T_k depends on all the previous coalescent times from T_{k+1} to T_n (see *e.g.* Wakeley (2009) for an extensive description of the coalescent).

In this paper, we derive a relationship between $N(t)$ and the distributions of the *cumulative* coalescent times, that we denote by V . More specifically, for $k \in [2, n]$:

$$V_k = T_n + \dots + T_k. \quad (1)$$

The V_k variables represent the sum of times from the present to each coalescent event. Because we only use the cumulative coalescent times V_k and not the individual times T_k , we refer to the times V_k for $k \in [2, n]$ as *coalescent times*, omitting the term *cumulative* for convenience. For example, the random variable V_2 represents the time to the Most Recent Common Ancestor (T_{MRCA}). All coalescent times V_k are expressed in generations. We denote by π_k the density function of V_k .

Polanski and colleagues (Polanski *et al.* 2003) derived the density function of coalescent times under varying population size as linear combinations of a set of functions $(q_j)_{2 \leq j \leq n}$, where

$$q_j(t) = \frac{\binom{j}{2}}{N(t)} \exp\left(-\binom{j}{2} \int_0^t \frac{1}{N(\sigma)} d\sigma\right). \quad (2)$$

Similar functions have previously been used in a context of varying population size (Griffiths and Tavaré 1994). For $k \in [2, n]$, the relationship between the density function π_k and $(q_j)_{2 \leq j \leq n}$ is

$$\pi_k(t) = \sum_{j=k}^n A_j^k q_j(t), \quad (3)$$

with

$$\begin{aligned} A_j^k &= \frac{\prod_{l=k, l \neq j}^n \binom{l}{2}}{\prod_{l=k, l \neq j}^n [\binom{l}{2} - \binom{l}{2}]}, \quad \text{for } k \leq j, \\ A_n^n &= 1 \\ A_j^k &= 0 \quad \text{for } k > j. \end{aligned} \quad (4)$$

We also define the integral of q_j with respect to t as

$$\begin{aligned} Q_j(t) &= \int_0^t q_j(u) du \\ &= 1 - \exp\left(-\binom{j}{2} \int_0^t \frac{1}{N(\sigma)} d\sigma\right). \end{aligned} \quad (5)$$

From equations 2 and 5 we can derive that:

$$N(t) = \binom{j}{2} \frac{1 - Q_j(t)}{q_j(t)}. \quad (6)$$

The principle of our method is to use the distributions of the coalescent times to get to the q_j functions. In other words, we invert the result of Polanski *et al.* (2003).

Theorem.

Given a sample of size n ,

$$q_j(t) = \sum_{k=j}^n B_k^j \pi_k(t),$$

with

$$\begin{aligned} B_k^j &= \frac{\binom{j}{2}}{\binom{k}{2}} \prod_{l=k+1}^n \left(1 - \frac{\binom{j}{2}}{\binom{l}{2}}\right), & \text{for } k < n, k \geq j, \\ B_k^j &= \frac{\binom{j}{2}}{\binom{k}{2}}, & \text{for } k = n \\ B_k^j &= 0 & \text{for } k < j \end{aligned}$$

Corollary

$$\begin{aligned} Q_j(t) &= \int_0^t q_j(u) du \\ &= \sum_{k=j}^n B_k^j \int_0^t \pi_k(u) du \\ &= \sum_{k=j}^n B_k^j \Pi_k(t) \end{aligned} \quad (7)$$

The proof of the theorem is given in the Appendix. This theorem implies that for any time t generations in the past, $q_j(t)$ and $Q_j(t)$ can be obtained using the distributions of coalescent times. From each q_j (and its integral Q_j), the function $N(t)$ can be obtained using equation 6. In contrast to the A_j^k coefficients (equation 4) which can become very large as n increases and are of alternate signs (Polanski *et al.* 2003), the B_k^j coefficients introduced in theorem are all positive and take values between 0 and 1 (Fig. 1). Thus, our formula is not constrained by numerical limitations and can be used for very large sample sizes.

Dealing with a finite number of observed gene-genealogies: adaptation of the theorem to time intervals, the “Popsicle”

The theorem states that the population size can be computed at any time in the past, provided that we know all the $n - 1$ distributions of coalescent times for any time in the past. However, this knowledge would require to observe the genealogies of an infinite number of independent loci evolving under the same N function over time. In practice, genomes are finite so we only have access to a finite number of loci to estimate the coalescent time distributions. We use empirical distribution functions $\hat{\Pi}_k(t)$ to estimate the cumulative distribution functions $\Pi_k(t)$ of the coalescent times as these estimators have good statistical properties: they are unbiased and asymptotically consistent (Van der Vaart 2000).

Because of the finite number of loci, time is discretized into intervals and $N(t)$ within each interval is estimated by its harmonic mean, as the harmonic mean of N has a simple relation-

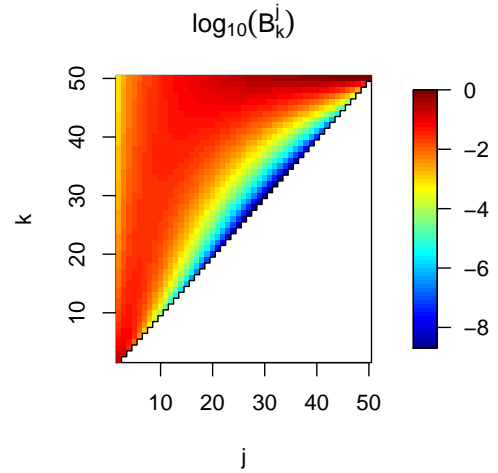


Figure 1 Heatmap of the values of $\log_{10}(B_k^j)$ for $n = 50$, as function of k and j . The white area represents the region where $B_k^j = 0$.

ship to the Q_j functions:

$$\begin{aligned} H_{[a,b]}(N) &= \frac{b-a}{\int_a^b 1/N(t) dt} \\ &= \frac{\int_0^b 1/N(t) dt - \int_0^a 1/N(t) dt}{b-a} \\ &= -\binom{j}{2} \frac{\int_0^b 1/N(t) dt + \binom{j}{2} \int_0^a 1/N(t) dt}{b-a} \\ &= -\binom{j}{2} \frac{\log(1 - Q_j(b)) - \log(1 - Q_j(a))}{b-a}. \end{aligned} \quad (8)$$

Definition (The Popsicle).

Given a sample of size n haploid individuals evolving in a random mating population of variable size N over time and given a number j between 2 and n , we define the **Population Size Coalescent-times based Estimator** (Popsicle) of N over a time interval $[a, b]$ to be:

$$\begin{aligned} \text{Popsicle}(N)_{[a,b]} &= \\ &= -\binom{j}{2} \frac{b-a}{\log(1 - \sum_{k=j}^n B_k^j \hat{\Pi}_k(b)) - \log(1 - \sum_{k=j}^n B_k^j \hat{\Pi}_k(a))}, \end{aligned}$$

with $\hat{\Pi}_k(t)$ being the empirical distribution function of the cumulative coalescent time variable V_k at time t .

In the rest of the paper, we set $j = 2$ (in equations 7 and 8), as it incorporates information from all coalescent time distributions and performs well even for very recent times (see Figs. S1, S2 and S3).

Quantifying the accuracy of the method

Let us consider a time discretization (t_0, t_1, \dots, t_m) , and define ARD and ARE as:

$$\text{ARD}_m = \frac{1}{m} \sum_{i=1}^m \frac{\hat{H}_{[t_{i-1}, t_i]}(N) - H_{[t_{i-1}, t_i]}(N)}{H_{[t_{i-1}, t_i]}(N)} \quad (9)$$

and

$$\text{ARE}_m = \frac{1}{m} \sum_{i=1}^m \frac{|\hat{H}_{[t_{i-1}, t_i]}(N) - H_{[t_{i-1}, t_i]}(N)|}{H_{[t_{i-1}, t_i]}(N)}, \quad (10)$$

where $\hat{H}_{[t_{i-1}, t_i]}(N)$ is the estimate of the harmonic mean of N during the time interval $[t_{i-1}, t_i]$ as defined in equation 8 with $j = 2$ and Q_2 replaced by its estimate \hat{Q}_2 , and $H_{[t_{i-1}, t_i]}(N)$ is the value for the true harmonic mean of N for the corresponding interval.

Algorithm for inferring gene-genealogies from polymorphism data

We apply a simple 2-step algorithm to infer gene-genealogies from polymorphism data. In the first step, we reconstruct the genealogy for each locus using the UPGMA algorithm and the matrix of pairwise differences. We convert the branch lengths from a time scale in mutations to a time scale in generations using the mutation rate per locus, which is considered known. Because of the discrete behavior of mutations, we do not have resolution for time intervals smaller than $1/(2L\mu)$ generations, with $L\mu$ being the total mutation rate of each locus. We discretize the time space into equal intervals of size $1/(2L\mu)$, starting at 0 and estimate the harmonic mean of N for each interval using the method. This strategy gives a first estimate of $N(t)$. In the second step, we refine our reconstruction by using the $N(t)$ profile computed in the first step. More precisely, we use the pairwise differences between haploid individuals/gene-copies to estimate the time to the most recent common ancestor of each pair of (haploid) individuals. From this computation, we construct a distance matrix on which we apply UPGMA to reconstruct the genealogy. We compute the coalescent times between the pairs of (haploid) individuals using a Gamma distribution, following the idea that if mutations are Poisson distributed onto the coalescent tree of a given pair of (haploid) individuals, and if the height of the tree is exponentially distributed with rate $1/N_e$ (which is the case under the constant model of $N(t) = N_e$), then the height of the tree T , conditional on the number of pairwise differences S between the two individuals, is Gamma distributed with shape $S + 1$ and with rate $2L\mu + 1/N_e$ [Tavaré et al. \(1997\)](#):

$$\begin{aligned} f_{T|S=s}(t) &\propto \mathbb{P}(S = s | T = t) f_T(t) \\ &\propto \frac{(2L\mu t)^s}{s!} e^{-2L\mu t} \times \frac{1}{N_e} e^{-\frac{t}{N_e}} \\ &\sim \Gamma(s + 1, 2L\mu + \frac{1}{N_e}). \end{aligned} \quad (11)$$

We use the first step to compute N_e as the harmonic mean of the inferred N from the present to the time interval corresponding to the number of observed differences between the two individuals.

Application to Human data

Data preparation. We use high coverage sequencing data from the 1000 Genomes Project, publicly available at <ftp://ftp.1000genomes.ebi.ac.uk/vol11/ftp/data/>. The

data is downloaded as VCF formatted files, from which we retain variant positions passing the filters set up by the 1000 Genomes Project, replacing the filtered out positions by missing genotypes. We retain only the trios and within each population existing in the sample, we phase the individuals using BEAGLE [Browning and Browning \(2007\)](#) under the trios file input option, but retain only the parents after phasing, as a sample of unrelated individuals. In doing the phasing, BEAGLE also imputes missing genotypes. We extract sequences corresponding to regions of supposedly no/low recombination as indicated by a recombination rate of 0 in the Decode genetic map [Kong et al. \(2002\)](#). The description of how those regions were ascertained is given below. We use the following population data: CEU (individuals of European ancestry from Utah, USA, sample size of 64), CHS (southern Han Chinese individuals, China, sample size of 56), PEL (Peruvian individuals from Lima, Peru, sample size of 58) and YRI (Yoruba individuals from Ibadan, Nigeria, sample size of 38).

Genetic map and no/low recombination regions. We use the Decode genetic map, which has been obtained by tracking more than 2,000 meioses in Islandic lineages [Kong et al. \(2002\)](#). The map is downloaded from the Table tool on the UCSC genome browser website [Genome Bioinformatics Group of UC Santa Cruz \(2013\)](#). We extract regions that have a recombination rate of 0. There are 22,321 such regions, of varying lengths (Fig. S10), with the most common length being 10kb (6,457 regions) and mean length being around 48kb. An alternative would be to use the HapMap recombination maps (which can be population specific), but since they are obtained using linkage disequilibrium (LD) information, which in turn is directly linked to demography and N , we focus on the Decode map. In particular regions of high LD can be suggestive of either a low local recombination rate, or a short gene-genealogy of the sample used for computing LD, or both. So, by extracting regions of low “recombination rate” in LD-based genetic maps, one might enrich the chosen regions in short gene-genealogies, leading to inference of a smaller population sizes. We see this effect when applying Popsicle to regions extracted using HapMapCEU with a total recombination threshold of 10^{-5} Morgans per region, although the difference of the $N(t)$ inference is relatively small between the different genetic maps (Fig. S11).

Comparison with PSMC and MSMC. Since its publication ([Li and Durbin 2011](#)), the PSMC method has been widely used to estimate past population size over time in a number of organisms. Thus, it is important to assess how our reconstruction methods compares to the results of PSMC as well as to the more recent iteration of this approach, MSMC ([Schiffels and Durbin 2013](#)). We use the sequences of the parents, with missing genotypes imputed by BEAGLE, and cut the sequences into regions of 100 base pairs, identical to the approach in the original paper. If no pairwise difference is observed within a region between the pairs of alleles at the 100 base pairs, the region is considered homozygote. If at least one pairwise difference is observed, the region is considered heterozygote. PSMC and MSMC are developed as a Hidden Markov Model, where the hidden states are the coalescent times of each region, while the observed states are the heterozygosity of the regions. It models recombination in the transition probabilities from one region to its neighbor. Intuitively, if a locus has many heterozygote regions, its underlying coalescent time is going to be inferred as large, whereas if a locus contains mostly homozygote regions, the coalescent time

is inferred as small. Chromosomes are given as independent sequences and only autosomes are used. For running PSMC, we use the same time intervals as the human study in the original PSMC paper. MSMC was used with the default time discretization, which is believed to be adapted for human data. Non-default parameters for MSMC were fixed recombination rate and a recombination to mutation ratio of 0.88.

Application of Popsicle. We apply Popsicle to the 22,321 low recombining regions for the 4 populations, under 2 different settings: in the first setting, we reconstruct an effective population size profile for every individual and average the results across all individuals from the same population (we refer to that setting as ‘Popsicle 1’); in the second setting, we use Popsicle on sub-samples of size 5 and compute the average of the obtained $N(t)$ estimates within each population (we refer to that setting as ‘Popsicle 5’). We use the 2-step procedure described above. Because PSMC also infers the local gene-genealogies when performing its MCMC computations, we also extracted the local gene-genealogies from PSMC’s decoding (option -d of the program) and apply Popsicle 1 to them. The results seem highly unstable, casting doubt on the reliability of the inferred local gene-genealogies from PSMC (see Fig. S11).

Data and code availability. Simulated data can be regenerated using the commands given in the Supporting Information. Data from the 1000 Genomes Project is available on the ftp server `ftp://ftp.1000genomes.ebi.ac.uk/vol1/ftp/`. Code for the computations is available at `jakobssonlab.iob.uu.se/popsicle/`.

Results

Evaluation of Popsicle on simulated gene-genealogies

Four different demographic scenarios. In order to evaluate the inference of $N(t)$, we used the software *ms* (Hudson 2002) to simulate samples under different population models with varying population size. We investigated 4 demographic scenarios illustrated in Fig. 2. The first 3 scenarios describe demographic models that span between the present and 100,000 generations in the past and that include various periods of constant population size, instantaneous changes, exponential growth or decline. In contrast to scenarios 1, 2 and 3, scenario 4 describes complicated changes in size that occur in the recent past, within the last 2,000 generations. Detailed descriptions of each scenario and the *ms* commands for the simulations are given in the Supporting Information (Section 2 and tables S1, S2, S3 and S4). In each studied scenario, we simulated 1,000,000 independent gene-genealogies of 20 haploid gene-copies (note that we will investigate the effect of number of loci and hence reduce that number for certain cases, see below). We assume that the true gene-genealogies are known and omit any inference of genealogies from polymorphism data at this stage. The genealogies were used to estimate coalescent time distributions and in turn reconstruct the population size profile using Popsicle. We discretized time into 100 equally long intervals (1,000 generations in each interval for scenarios 1, 2 and 3, and 20 generations in each interval for scenario 4).

The harmonic mean estimates are very close to the true size in all 4 scenarios, with better accuracy in the recent past than in the distant past (Fig. 2). The division of time into 100 intervals is arbitrary and dividing time using the true break points

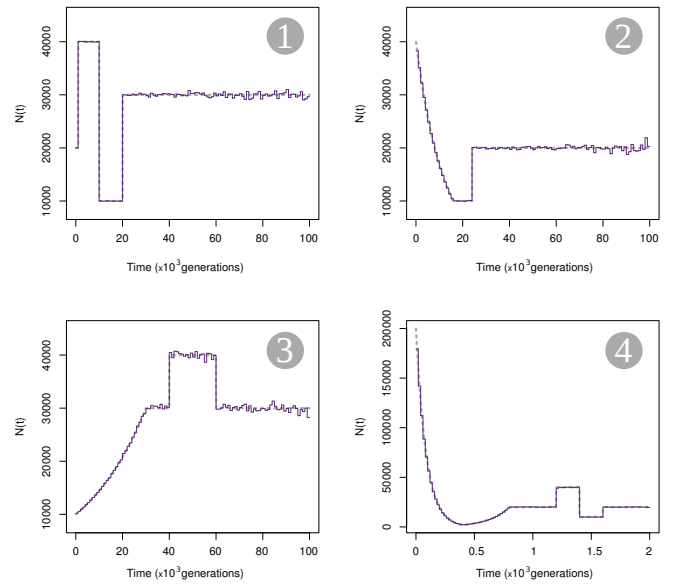


Figure 2 Estimation of N based on simulated gene-genealogies. Four scenarios of variable population sizes are used to generate 1,000,000 independent loci in each scenario, for a sample of size 20 (10 diploid individuals). Time is divided into 100 regular intervals and estimates of the harmonic mean of N (purple solid lines) for all intervals are plotted. The true values of N over time are indicated by gray dashed lines.

of the scenarios leads to an almost perfect fit for the time periods where the population size is constant, whereas dividing time more finely in the periods of variable size improves the estimation, as long as there are enough coalescent times occurring within the interval to get a good estimate of the cumulative distribution function (results not shown). The $N(t)$ estimation is very accurate in periods of small population size, especially when it is followed by an expansion. Estimates of $N(t)$ are more variable around the true value when population size was larger in the past (scenario 3). These observations can be understood intuitively by the fact that $\pi(t)$ will be better estimated in time-periods of small N as the coalescence rate is proportional to the inverse of N . The resolution of the reconstruction method for N is also accurate in the recent past, even for drastic or rapid changes in size over a couple of hundred generations (scenario 4). In summary, with a finite but sufficiently large number of loci to estimate the cumulative distributions of coalescent times, we can accurately reconstruct the global shape of the population size over time, from very recent times to far into the past.

Effect of sample size. We tested the accuracy of our method for different sample sizes. To be able to quantify the performance in reconstructing the population size over time, we introduced two statistics: the *average relative difference* (ARD), and the *average relative error* (ARE). The former quantifies a systematic deviation from the true value of the population size, while the latter quantifies the error of the estimation (see Methods section for the computation of ARD and ARE). We used scenarios 1 and 4, from which we simulated 1,000,000 independent gene-genealogies with sample sizes taken from the values {2, 5, 10, 15, 20, 30}. Each scenario was divided into large periods, to be able to discriminate the effect of sample size in the $N(t)$ reconstruction between recent and old time periods and

between periods of large and small population sizes. Scenario 1 was divided into 5 periods, while scenario 4 was divided into 6 periods (table 1, Fig. 3). Within each period, we discretized the time into 100 equally long intervals and assessed the $N(t)$ reconstruction with ARD and ARE (Fig. 3).

Period	Scenario	
	1	4
1	[0-1,000]	[0-400]
2	[1,000-10,000]	[400-800]
3	[10,000-20,000]	[800-1,200]
4	[20,000-60,000]	[1,200-1,400]
5	[60,000-100,000]	[1,400-1,600]
6	-	[1,600-2,000]

Table 1 Division of scenarios 1 and 4. Time intervals are given in generations.

In general, scenario 1 is predicted more accurately than scenario 4, with an average relative error ranging between 0.2% and 3.6% compared to a range of 0.4% to 12.1% for scenario 4. There is little bias in the reconstruction of the 2 scenarios, except maybe for sample of size 2 in scenario 4, where there may be an upward bias of some 5% in period 4. In both scenarios and in all periods, the accuracy of the estimates are improved by increasing the sample size. The improvement is substantial when increasing the sample size from 2 to 10 and increasing the sample size further only results in modest improvements. Note the relatively higher error for the instantaneous population expansion of scenario 4 (period 4), irrespective of sample size, suggesting that a large population size for a brief period of time is difficult to infer. Accurate estimates of N for such periods require a greater number of loci to obtain resolution on par with time-periods with smaller N , as the number of coalescences is reduced for periods of large N . This effect is investigated further in the next section.

Effect of the number of loci. With the full knowledge of the density functions π_k , we could potentially compute N at any time in the past. However, in practice, the distributions can only be estimated where observations are made, hence we are limited to the time ranges where reasonable estimates of the distributions can be computed because we have enough observations. For that reason, the more loci, the more coalescent times can be observed within a time interval and the better the estimate of the cumulative distributions. Here we investigate the robustness of Popsicle to varying number of loci, by simulating genealogies of samples of size 20 under scenarios 1 and 4. We compare the effect of the number of loci for different periods in the past, as described in table 1, divide each period into 100 regular intervals on which we estimate the harmonic mean of N and measure the accuracy within each period with ARD and ARE.

The accuracy of the N estimates in all periods for both scenarios increases with increasing number of loci (fig. 4). Generally, for these investigated (and human realistic) scenarios, the average relative error (ARE) and the average relative difference

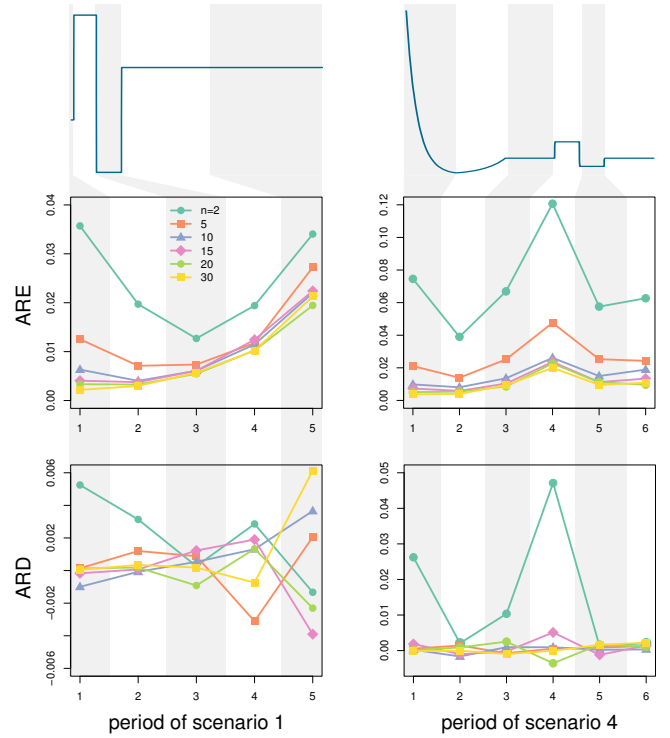


Figure 3 Effect of sample size. We divide scenario 1 (left panel) and scenario 4 (right panel) into smaller periods of time where we assess the average relative error and the average relative difference on the N estimates compared to the true values of N , as functions of the sample size used for the estimation. 1,000,000 loci were simulated for each scenario and each sample size. The original scaling for the x and y axis of both scenarios can be found in Fig. 2.

(ARD) from the true values are low for cases with 50,000 loci ($ARE < 0.1$, $ARD < 0.02$), and still moderate for 10,000 loci ($ARE < 0.3$, $ARD < 0.2$). For smaller numbers of loci, errors can reach 40% and more. For scenario 1 and 1,000 loci, no coalescence occurred during periods 4 and 5 in any of the simulations, making the inference impossible for these periods. Similarly, there were no coalescence events in period 5 of scenario 1 with 5,000 loci, as well as periods 4 and 6 in scenario 4 with 1,000 loci. This illustrates the greater difficulty of accurate N reconstruction for older time-periods (in particular if the period is preceded by a severe bottleneck), and periods of large population size, both subject to low probabilities of coalescences to occur. Thus, depending on the history of the population and how far back in time N is of interest, the required number of loci will vary. Sub-sampling from some particular number of loci might give an idea on whether or not a particular number of loci is enough for a good estimation of $N(t)$.

Effect of recombination. We explore the robustness of the $N(t)$ reconstruction if recombination occurs in the loci, but when each locus is treated as non-recombining. This case is equivalent to consider the entire sequence fragment as non-recombining and having a single underlying genealogy, represented by an average tree, instead of considering the multiple underlying genealogies within the (recombining) locus. We investigate the effect of ignoring recombination for samples of size 2 and for

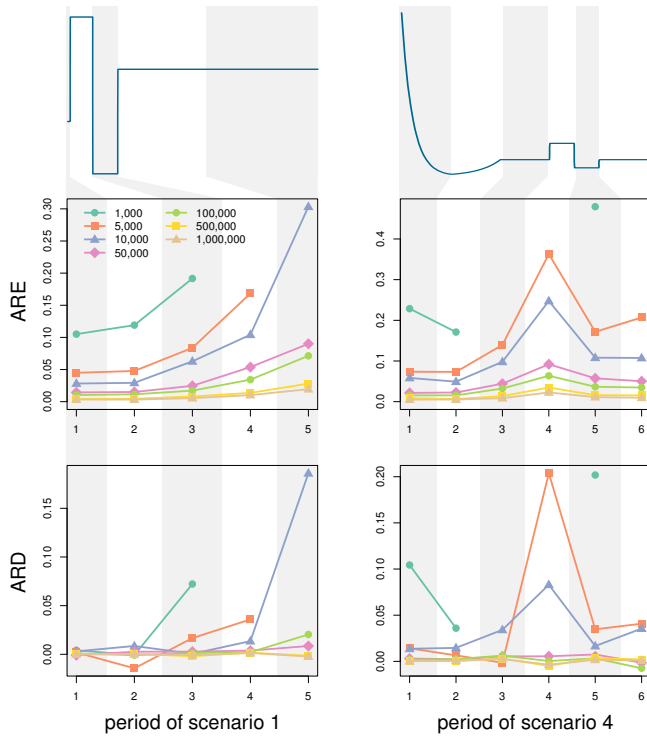


Figure 4 Effect of the number of loci. We divide scenario 1 (left panel) and scenario 4 (right panel) into smaller periods of time where we assess the average relative error (ARE) and the average relative difference (ARD) on the N estimates compared to the true values of N , as functions of the number of loci used for the estimation. The sample size for all simulations is 20. The original scaling for the x and y axis of both scenarios can be found in figure 2.

samples of size 20, for different levels of recombination within each simulated locus. For a sample of size 2, the average tree is simply the weighted mean of the trees of the non-recombining segments, with the weight being the relative length of each non-recombining segment compared to the total segment length. For the case of 20 gene copies, we build the “average tree” by applying a UPGMA algorithm to the weighted average matrix of pairwise time to coalescence between all pairs of haploid individuals. We use scenarios 1 and 4, as well as the constant size model, to study the robustness of the method to different levels of recombination. We tested 5 levels of recombination within the locus: 10^{-6} , 5×10^{-6} , 10^{-5} , 5×10^{-5} and 10^{-4} . Assuming a recombination rate of 1.25×10^{-8} per site per generation, which is around the estimated average for the human recombination rate, these 5 levels represent loci of length 80, 400, 800, 4,000 and 8,000 base pairs.

Cryptic recombination can lead to inference of spurious changes in population size, even under the simple model of constant population size (Fig. 5), although the effect is limited to a factor of at most ~ 2 in the investigated cases. For instance, scenarios 1 and 4 that are relatively realistic for e.g. humans show low to moderate bias due to cryptic recombination, even for the cases of high levels of recombination (or long fragments). Overall, the effect of cryptic recombination appears to be indifferent to sample size. For the case of

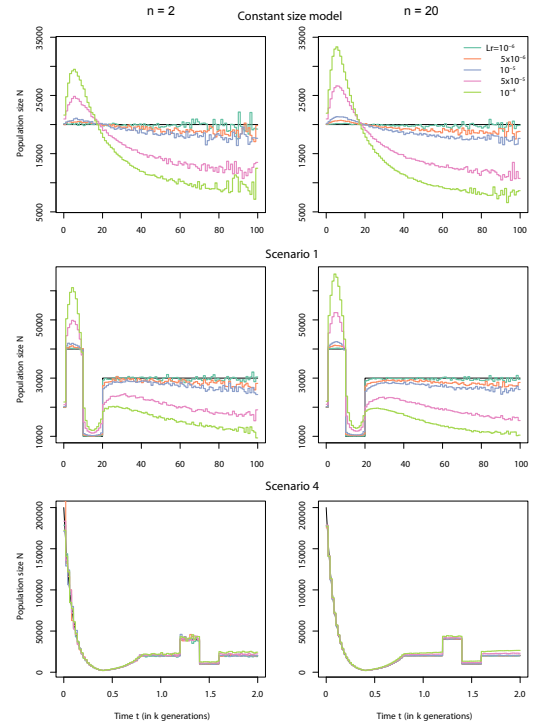


Figure 5 Effect of omitting recombination. Comparison between $N(t)$ reconstructed using gene-genealogies computed as a weighted average of the gene-genealogies obtained from ms and true $N(t)$ (black lines) under three different demographic scenarios. We generated 1,000,000 independent loci for two different sample sizes, 2 and 20 haploid gene-copies, and for 5 different levels of recombination within each locus. The three different demographic scenarios were: the constant size model (top), scenario 1 (middle) and scenario 4 (bottom). The different cryptic recombination rates for each locus (in Morgan) is indicated by different colors and the values of the recombination of the segments are given in the legend.

constant size, we can provide some intuition on the effects of cryptic recombination. We note that genealogies inferred from recombining loci are weighted averages of the underlying genealogies of the non-recombining fragments of the loci, and therefore tend to be more star-like as well as of intermediate size. Estimating one single gene-genealogy from such a mosaic of correlated gene-genealogies will have an impact on the distributions of coalescent times (see Fig. S5). Star-like gene-genealogies are typically associated with rapid and recent expansions, which is what the inferred $N(t)$ shows in the case of constant population size and high level of cryptic recombination.

Towards solving the full inference problem

Popsicle is designed to infer effective population size over time from samples of gene-genealogies obtained under the demographic model studied, and not directly from observed sequence data. However, to provide an illustration and one example of a solution to integrate Popsicle into a full inference method that would take sequence data as input, we outline one heuristic approach here. This approach builds local gene-genealogies from sequence data and applies Popsicle to the distributions of coalescent times obtained using inferred gene-genealogies.

Our aim is notably to apply this full resolution method on human sequences, to be able to compare these population size profiles to previously published results. Hence, we have to find a way to obtain the gene-genealogies from sequence data. One way could be to use *ARGWeaver* (Rasmussen *et al.* 2014), as is done in Palacios *et al.* (2015). However, Palacios *et al.* (2015) found a systematic bias in their reconstruction of effective population size over time profiles when using *ARGWeaver* to infer gene-genealogies, even for rather simple demographic scenarios. Here, we develop a simple 2-step algorithm based on UPGMA and properties of the coalescent to infer gene-genealogies from sequences, as it seemed to perform well on simulated non-recombining sequences. A detailed outline of the algorithm is described in the Methods section. Inferring gene-genealogies from sequences is a challenging problem, especially for recombining sequences, and we note that our algorithm is merely a heuristic solution to the problem that performs well.

We evaluate our ability to reconstruct the population size over time using Popsicle together with our algorithm to infer gene-genealogies. In particular, we study the impact of the mutation rate on the reconstruction, to get a sense on how large the mutation rate needs to be to obtain reasonable results. We present the results for samples of size 20, simulated with values of $L\mu$ taken from $\{10^{-4}, 5 \times 10^{-4}, 10^{-3}, 5 \times 10^{-3}, 10^{-2}\}$, for 1,000,000 non recombining loci and under scenarios 1 and 4 (Fig. 6 and S7 Fig). For reference, with a mutation rate of 1.25×10^{-8} per base pair per generation, the range of $L\mu$ values corresponds to loci of 8, 40, 80, 400 and 800 kb respectively. With a mutation rate $L\mu$ of 5×10^{-4} , we can already uncover a good estimate of the population size profile. Unsurprisingly, the more mutations there are, the better the estimates of times to coalescence and the more accurate the reconstruction. This fact is particularly important for recent times where enough mutations are required to accumulate to infer the very recent population sizes (Fig. S6).

Application to human sequence data

We apply the developed heuristic algorithm of gene-genealogies inference followed by Popsicle to empirical sequence data. The effect of recombination can be mitigated by considering only regions of the genome with low or no recombination, provided that we have access to a good genetic map. Following this principle, we applied Popsicle to human genome sequence data from the 1000 Genomes Project (Complete Genomics high coverage samples from the (Complete Genomics data from 1000 Genomes public repository 2013)), for Yoruba individuals from Nigeria, for American individuals of European ancestry from Utah, U.S.A, for Han Chinese individuals from southern China and for Peruvian individuals. We extracted regions of no recombination according to the Decode recombination map (Kong *et al.* 2002) (see Methods section for a description of the data preparation). For comparison, we also use PSMC (Li and Durbin 2011) and MSMC (Schiffels and Durbin 2013) to infer $N(t)$ profiles from the data. We inferred $N(t)$ profiles for the 4 populations in two ways: a) using single individuals (as PSMC does) and averaging across single individuals (denoted 'Popsicle 1'), and b) using 5 individuals from the population (denoted 'Popsicle 5'). From simulations, we have observed that more than 10 haploid sequences only results in a minor improvement of the inference in population size (see fig. 3).

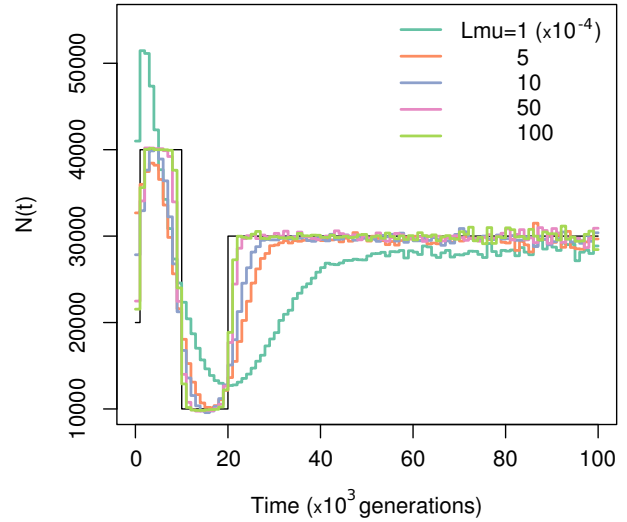


Figure 6 Effect of estimating gene-genealogies from polymorphism data. Reconstruction of $N(t)$ from distributions of coalescent times computed from gene-genealogies inferred from polymorphism data. We used a sample size of 20 and 1,000,000 independent loci, evolving under scenario 1. The mutation rate per locus $L\mu$ is indicated by the color of the line and the legend gives the mutation rates.

Overall, the Popsicle profiles of effective population size in the last million years for every population largely resemble the vague knowledge about past human population sizes as well as the $N(t)$ profiles inferred by *e.g.* PSMC (Fig. 7A). In contrast, the profile reconstructed by MSMC is very different than PSMC and Popsicle. As MSMC only traces the first coalescent even between any pair of the ten chromosomes in the data, it provides estimates of the population size only for the last 50,000 years or so. A comparison on log-scale between the three methods applied to CEU data is provided in Fig. S7. Results of MSMC and PSMC across populations are given in Fig. S8 and Fig. S9 respectively.

Popsicle reveals a steady but slow increase in effective population size starting around 1 million years ago, reaching a maximum between 200,000 and 500,000 years ago, followed by a sharper decline and a recovery during the last 100,000 years for European and East Asian populations. However, prior to a million years ago, the population size inferred by PSMC is higher than the population size inferred by Popsicle (Fig. S7). In addition, Popsicle infers a less sharp decline in population size than PSMC does, for all four populations, and infers a population size history markedly different for Yoruba compared to the three other non-African populations (Fig. 7B and Fig. 7C) whereas the Yoruban population follows the non-African populations rather closely in the PSMC results (Fig. S9). Popsicle results suggest a somewhat larger ancestral population for Yoruba than the ancestral population size of the 3 non-African populations, which could be interpreted as deep and long-lasting population structure within Africa between 400,000 and 100,000 years ago. Note however that the

non-recombining regions have been chosen using the Decode recombination map, a genetic map formed by tracking more than 2,000 meioses in Icelandic lineages. Recombination patterns and hotspots in particular are believed to be variable across populations (Myers *et al.* 2005; Baudat *et al.* 2010), thus the non-recombining regions selected using the Decode map might be in fact recombining in Yoruba, resulting in a bias of the population size estimates (see Fig. 5). Recombination maps for Yoruba have been computed (Frazer *et al.* 2007), but because they have been inferred using properties of linkage disequilibrium which itself depends on demography, they would not be ideal to use for selecting regions of low/no recombination. A future pedigree- or sperm-typing-based recombination map for the Yoruba would help in understanding the differently inferred $N(t)$ profiles for African and non-African populations.

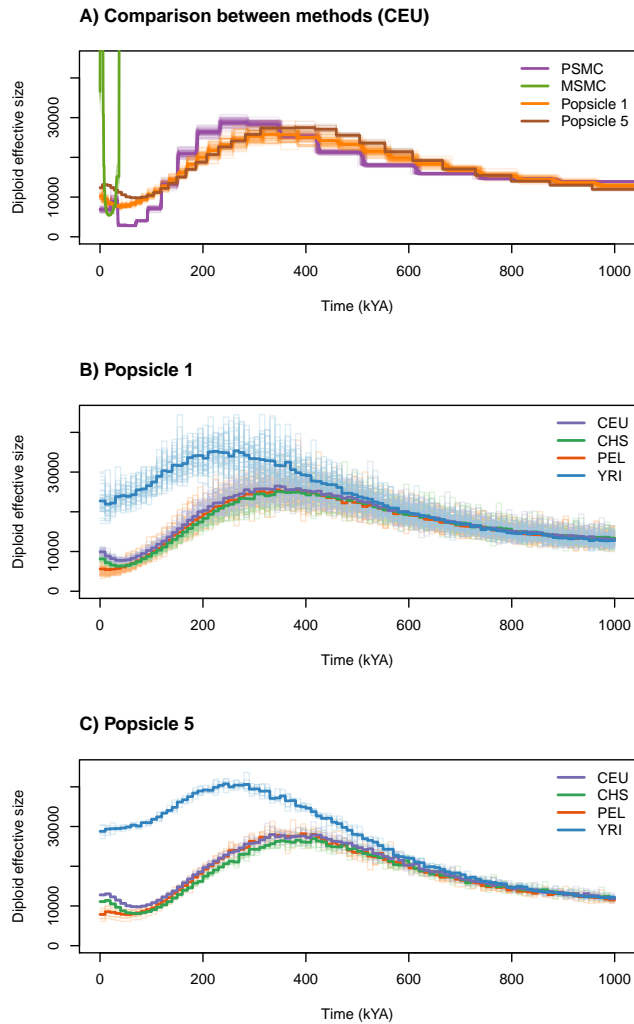


Figure 7 Comparison of $N(t)$ inference among different methods. A) Comparison of $N(t)$ profiles inferred using PSMC, MSMC, Popsicle 1 and Popsicle 5; B) Inferred $N(t)$ profiles for four populations, CEU, CHS, PEL, and YRI based on Popsicle 1; C) Inferred $N(t)$ profiles for four populations, CEU, CHS, PEL, and YRI based on Popsicle 5. The time scale is computed assuming a mutation rate of 1.25×10^{-8} and a generation time of 25 years.

Popsicle 1 and Popsicle 5 give similar effective population size profiles (Fig. 7B and 7C) but the time of the major features in Popsicle 5 are shifted to older times compared to Popsicle 1. Whereas Popsicle 1 suggests a bottleneck in non-African populations that reaches its strongest effect between 30,000 and 40,000 years ago, Popsicle 5 places the bottleneck between 70,000 and 80,000 years ago, which is more in line with the estimates of timing of the founder effects due to a dispersal out-of-Africa (Sally and Durbin 2012). In neither Popsicle nor PSMC do we see the super-exponential increase in size that has occurred in all populations since the spread of agriculture (Keinan and Clark 2012), but we possibly do in the MSMC results (Fig. S8). It is possible that for Popsicle and PSMC too few loci are included for a reliable inference in the recent times, too few individuals, or that the mutation rate per locus is too low to observe a dramatic expansion in population size (as most terminal branches will be very short in genealogies from models of rapid recent expansion). Keinan and Clark (2012) suggest that observing enough rare variants is necessary to infer the exponential growth that human populations have been going through in the past thousands of years.

The resolution of Popsicle can be better than that of PSMC, as Popsicle does not constrain the coalescent times into a finite (and usually rather small) set of values like PSMC does. In principle, any time discretization for computing the harmonic mean of the effective population size over time can be used, though in practice we need to make sure that there are enough coalescences within each time interval to get reliable estimates of the effective size. Popsicle is also markedly faster than PSMC, not only because it uses a moderate number of non-recombining regions, but also because of the closed form relationship between population size and coalescent time distributions. Most of the computational time is spent on inferring the gene-genealogies (which takes less than 20 minutes for the 22,321 loci in the data application). Once the gene-genealogies are computed, the application of the theorem for reconstructing the population size takes a few seconds. Finally, Popsicle accommodates samples of any size, which should lead to more reliable results, especially in the recent times, provided that the phasing of the genomes is accurate.

Applying Popsicle to extracted regions of limited recombination should not bias the results in principle. Regardless of the molecular reason explaining the low rate of recombination in the region (for instance, limited access for crossovers or conservation constraints due to functional importance of the region), the fact that there is one local gene-genealogy for the entire region is what matters for the method to work. However for applications to empirical data, variation in the local mutation rate, due to purifying selection for example, will affect the reconstruction of the gene-genealogy by changing the estimates of the branch lengths for different loci. This could potentially cause bias in the reconstructed Popsicle profiles, as all gene-genealogies are inferred using one mutation rate. Using a mutation map obtained from the study of *de novo* mutations in trios or pedigrees could alleviate this issue and infer the local gene-genealogies from genetic data using a specific mutation rate for each region.

Discussion

The major implication of our main result is to reduce the problem of $N(t)$ reconstruction from polymorphism data to a problem

of gene-genealogy inference. If local gene-genealogies in the genome can be inferred accurately from observed polymorphism data, then our theorem can be used to estimate $N(t)$ with great accuracy as well. Currently, however, local gene-genealogy inference remains a challenge. First, most genomes do not consist in large sets of independent non-recombining loci, but rather in sets of recombining chromosomes. Each chromosome can be seen as a linear structure of successive non-recombining loci whose underlying genealogies are correlated with one another. This correlation decays with distance between loci due to recombination. Also, in a given sample, the exact positions on the chromosome of the recombination events, hence the break points between the non-recombining bits of DNA, are unknown. Fully recovering the genealogies along the chromosome means reconstructing the ancestral recombination graph from polymorphism data and this is a challenging problem (Griffiths and Marjoram 1996; McVean and Cardin 2005; Parida *et al.* 2008; Zheng *et al.* 2014; Rasmussen *et al.* 2014). We noted based on simulations that a low to moderate level of cryptic (unaccounted) recombination lead to accurate estimates of $N(t)$, but the bias increase with greater levels of cryptic recombination.

The problem of inferring gene-genealogies can also be challenged by a lack of mutation events to accurately estimate coalescent times. For some species, there might not be enough mutation events to be able to infer the local gene-genealogies of non-recombining segments. In humans for example, the ratio between the mutation rate per site and per generation and the recombination rate per site and per generation is likely close to 1 (or 2, depending on assumptions on mutation rate; the pedigree based mutation rate or the divergence based mutation rate, see *e.g.* Scally and Durbin (2012)). Hence, on average, for each mutation observed locally in a sample, there is also a recombination break-point nearby. A targeted approach, where only low recombining regions of sufficient length, are considered could yield better results and we have shown that such strategy can provide $N(t)$ profiles that are similar to estimates based on approaches that specifically model recombination. These challenges are inherent to the problem of estimating local gene-genealogies from sequence data. There has been interesting developments in this area (see *e.g.* Rasmussen *et al.* 2014), and we look forward to the further methodological improvements to infer the ancestral recombination graph.

In order to gauge some intuition of usefulness of Popsicle for human genome data, we can make a computation of the number of regions that can be recruited for analysis. Assume a genome of 3 billion bp, a mutation rate of 1.25×10^{-8} per bp and generation, a recombination rate of 1.25×10^{-8} per bp and generation, and an effective population size of 10,000 diploid individuals. Assume further that the genome is organized into recombination “hot-spot” and “cold-regions”, where the former account for 99% of the recombination events and the “cold-regions” have a 100 times lower recombination rate compared to the genome average. Assuming an average “cold-region” extends for 40 kbp (compare with fig. S10), the average recombination rate in such a locus is 5×10^{-6} (orange line in Fig. 5) and the average number of pairwise mutations would be 20. Hence, the genome would consist of 75,000 genome regions of length 40kbp that contain abundant polymorphism data to obtain a good estimate of gene-genealogies. This rough computation illustrates that at least the human genome harbor favorable properties that Popsicle can utilize.

We present a novel method for inferring population size over time, a problem that has recently gained much interest due to the availability of genome sequence data. By analytically solving the relationship between $N(t)$ and the distribution of coalescent times, we have connected $N(t)$ to the problem of inferring the ancestral recombination graph from polymorphism data, which remains a challenge in population genetics. We show that, using a moderate number of loci and a simple algorithm for genealogy inference, our method Popsicle was able to recover the general pattern of population size as a function of time with high resolution and using modest computational time, properties that will be useful for future large-scale studies of many full genomes.

Acknowledgments

We thank Martin Lascoux and Michael G. B. Blum for helpful comments on the manuscript. This work was supported by grants to MJ from the Knut and Alice Wallenberg foundation, the Swedish Research Council (no. 642-2013-8019), and the Göran Gustavsson foundation.

Literature Cited

- Baudat, F., J. Buard, C. Grey, A. Fledel-Alon, C. Ober, M. Przeworski, G. Coop, and B. De Massy, 2010 Prdm9 is a major determinant of meiotic recombination hotspots in humans and mice. *Science* **327**: 836–840.
- Boserup, E., 1981 *Population and technological change: A study of long-term trends*. University of Chicago Press Chicago Ill. United States 1981.
- Browning, S. R. and B. L. Browning, 2007 Rapid and accurate haplotype phasing and missing-data inference for whole-genome association studies by use of localized haplotype clustering. *The American Journal of Human Genetics* **81**: 1084–1097.
- Cohen, J. E., 1995 How many people can the earth support? *The Sciences* **35**: 18–23.
- Complete Genomics data from 1000 Genomes public repository, 2013 File location for Complete Genomics high coverage data. ftp://ftp.1000genomes.ebi.ac.uk/vol1/ftp/complete_genomics_indices/20130820_cg_data.index, Accessed: 2013-09-30.
- Drummond, A. J., M. A. Suchard, D. Xie, and A. Rambaut, 2012 Bayesian phylogenetics with beauti and the beast 1.7. *Molecular Biology and Evolution* **29**: 1969–1973.
- Frazer, K. A., D. G. Ballinger, D. R. Cox, D. A. Hinds, L. L. Stuve, R. A. Gibbs, J. W. Belmont, A. Boudreau, P. Hardenbol, S. M. Leal, *et al.*, 2007 A second generation human haplotype map of over 3.1 million snps. *Nature* **449**: 851–861.
- Genome Bioinformatics Group of UC Santa Cruz, 2013 Genome Browser Table Tool. http://genome-euro.ucsc.edu/cgi-bin/hgTables?hgid=208520476_rAHGRV4HFcmGAOng8Gp4ETNO9vYF.
- Griffiths, R. C. and P. Marjoram, 1996 Ancestral inference from samples of dna sequences with recombination. *Journal of Computational Biology* **3**: 479–502.
- Griffiths, R. C. and S. Tavaré, 1994 Sampling theory for neutral alleles in a varying environment. *Philosophical Transactions of the Royal Society B: Biological Sciences* **344**: 403–410.
- Ho, S. Y. W. and B. Shapiro, 2011 Skyline-plot methods for estimating demographic history from nucleotide sequences. *Molecular Ecology Resources* **11**: 423–434.
- Hudson, R. R., 2002 Generating samples under a Wright-Fisher neutral model of genetic variation. *Bioinformatics* **18**: 337–338.

- Jakobsson, M., S. W. Scholz, P. Scheet, J. R. Gibbs, J. M. VanLiere, H. . Fung, Z. A. Szpiech, J. H. Degnan, K. Wang, R. Guerreiro, J. M. Bras, J. C. Schymick, D. G. Hernandez, B. J. Traynor, J. Simon-Sanchez, M. Matarin, A. Britton, J. Van De Leemput, I. Rafferty, M. Bucan, H. M. Cann, J. A. Hardy, N. A. Rosenberg, and A. B. Singleton, 2008 Genotype, haplotype and copy-number variation in worldwide human populations. *Nature* **451**: 998–1003.
- Keinan, A. and A. G. Clark, 2012 Recent explosive human population growth has resulted in an excess of rare genetic variants. *science* **336**: 740–743.
- Kong, A., D. F. Gudbjartsson, J. Sainz, G. M. Jonsdottir, S. A. Gudjonsson, B. Richardsson, S. Sigurdardottir, J. Barnard, B. Hallbeck, G. Masson, *et al.*, 2002 A high-resolution recombination map of the human genome. *Nature genetics* **31**: 241–247.
- Lahr, M. M. and R. Foley, 2001 Genes, fossils and behaviour: when and where do they fit. In *Genes, fossils, and behaviour: an integrated approach to human evolution*, edited by P. Donnelly and R. Foley, volume 310, pp. 13–48, IOS press, Amsterdam, Netherlands.
- Li, H. and R. Durbin, 2011 Inference of human population history from individual whole-genome sequences. *Nature* **475**: 493–U84.
- Li, J., H. Li, M. Jakobsson, S. Li, P. Sjodin, and M. Lascoux, 2012 Joint analysis of demography and selection in population genetics: where do we stand and where could we go? *Molecular Ecology* **21**: 28–44.
- Lindblad-Toh, K., C. M. Wade, T. S. Mikkelsen, E. K. Karlsson, D. B. Jaffe, M. Kamal, M. Clamp, J. L. Chang, E. J. Kulbokas, M. C. Zody, E. Mauceli, X. Xie, M. Breen, R. K. Wayne, E. A. Ostrander, C. P. Ponting, F. Galibert, D. R. Smith, P. J. deJong, E. Kirkness, P. Alvarez, T. Biagi, W. Brockman, J. Butler, C.-W. Chin, A. Cook, J. Cuff, M. J. Daly, D. DeCaprio, S. Gnerre, M. Grabherr, M. Kellis, M. Kleber, C. Bardeleben, L. Goodstadt, A. Heger, C. Hitte, L. Kim, K.-P. Koepfli, H. G. Parker, J. P. Pollinger, S. M. J. Searle, N. B. Sutter, R. Thomas, C. Weber, and E. S. Lander, 2005 Genome sequence, comparative analysis and haplotype structure of the domestic dog. *Nature* **438**: 803–819.
- Marjoram, P. and J. D. Wall, 2006 Fast" coalescent" simulation. *BMC genetics* **7**: 1.
- McVean, G. A. T. and N. J. Cardin, 2005 Approximating the coalescent with recombination. *Phil. Trans. R. Soc. B* **360**: 1387–1393.
- Myers, S., L. Bottolo, C. Freeman, G. McVean, and P. Donnelly, 2005 A fine-scale map of recombination rates and hotspots across the human genome. *Science* **310**: 321–324.
- Nielsen, R., 2005 Molecular signatures of natural selection. *Annu. Rev. Genet.* **39**: 197–218.
- Palacios, J. A., J. Wakeley, and S. Ramachandran, 2015 Bayesian Nonparametric Inference of Population Size Changes from Sequential Genealogies. *GENETICS* **201**: 281+.
- Palkopoulou, E., L. Dalén, A. M. Lister, S. Vartanyan, M. Sablin, A. Sher, V. N. Edmark, M. D. Brandström, M. Germonpré, I. Barnes, *et al.*, 2013 Holarctic genetic structure and range dynamics in the woolly mammoth. *Proceedings of the Royal Society B: Biological Sciences* **280**: 20131910.
- Parida, L., M. Melé, F. Calafell, and J. Bertranpetit, 2008 Estimating the ancestral recombinations graph (arg) as compatible networks of snp patterns. *Journal of Computational Biology* **15**: 1133–1153.
- Polanski, A., A. Bobrowski, and M. Kimmel, 2003 A note on distributions of times to coalescence, under time-dependent population size. *Theoretical Population Biology* **63**: 33–40.
- Ramachandran, S., O. Deshpande, C. C. Roseman, N. A. Rosenberg, M. W. Feldman, and L. L. Cavalli-Sforza, 2005 Support from the relationship of genetic and geographic distance in human populations for a serial founder effect originating in Africa. *Proc. Natl. Acad. Sci. USA* **102**: 15942–15947.
- Rasmussen, M. D., M. J. Hubisz, I. Gronau, and A. Siepel, 2014 Genome-wide inference of ancestral recombination graphs. *PLoS Genetics* **10**: e1004342.
- Scally, A. and R. Durbin, 2012 Revising the human mutation rate: implications for understanding human evolution. *Nature Reviews Genetics* **13**: 745–753.
- Schiffels, S. and R. Durbin, 2013 Inferring human population size and separation history from multiple genome sequences. *Nature Genetics* **46**: 919–925.
- Sheehan, S., K. Harris, and Y. S. Song, 2013 Estimating variable effective population sizes from multiple genomes: A sequentially markov conditional sampling distribution approach. *Genetics* **194**: 647–662.
- Tavaré, S., D. J. Balding, R. C. Griffiths, and P. Donnelly, 1997 Inferring coalescence times from dna sequence data. *Genetics* **145**: 505–518.
- Van der Vaart, A. W., 2000 *Asymptotic statistics*, volume 3. Cambridge university press.
- Wakeley, J., 2009 *Coalescent Theory: an introduction*. Roberts and company Publishers.
- Zheng, C., M. K. Kuhner, and E. A. Thompson, 2014 Bayesian inference of local trees along chromosomes by the sequential markov coalescent. *Journal of molecular evolution* **78**: 279–292.

Appendix

Derivation of the B_k^j

The relationship between the density function of the cumulative coalescent times π_k and the family of functions q_j can be written in matrix form. We define $\vec{\pi}(t)$ the vector of density functions of cumulative coalescent times $(\pi_2(t), \dots, \pi_n(t))$, $\vec{q}(t)$ the vector $(q_2(t), \dots, q_n(t))$ and the upper triangular matrix $\mathbf{A} = (A_{ij})_{2 \leq i, j \leq n} = (A_j^i)_{2 \leq i, j \leq n}$. Then from equation 3, from Polanski *et al.* (2003) we have

$$\vec{\pi}(t) = \mathbf{A} \vec{q}(t)$$

To prove that the B_k^j defined in theorem can invert the relationship between $\pi_k(t)$ and $q_j(t)$, we show that the matrix \mathbf{B} defined by $(B_{ij})_{2 \leq i, j \leq n} = (B_j^i)_{2 \leq i, j \leq n}$ is the inverse matrix of \mathbf{A} . We define $\mathbf{C} = (C_{ij})_{2 \leq i, j \leq n} = \mathbf{A} \times \mathbf{B}$. Our aim is to prove that \mathbf{C} is in fact the identity matrix. First, we know that \mathbf{C} is an upper triangular matrix, as both \mathbf{A} and \mathbf{B} are upper triangular matrices. To prove that \mathbf{C} is the identity matrix, we cover 4 separate cases: C_{in} for $2 \leq i < n$, C_{ij} for $2 \leq i < j < n$, C_{ii} for $2 \leq i < n$ and finally C_{nn} . For the computation of the two first cases, we need to introduce a notation:

$$F_{i,j,n} = \prod_{l=i, l \neq j}^n \frac{1}{\binom{l}{2} - \binom{j}{2}} \quad (12)$$

We know from partial fraction decomposition that

$$\begin{aligned} F_{i,j,n} &= (-1) \sum_{l=i, l \neq j}^n \prod_{m=i, m \neq l}^n \frac{1}{\binom{m}{2} - \binom{l}{2}} \\ &= (-1) \sum_{l=i, l \neq j}^n F_{i,l,n}. \end{aligned} \quad (13)$$

We compute the coefficients C_{in} , for $2 \leq i < n$:

$$\begin{aligned} C_{in} &= \sum_{k=2}^n A_{ik} B_{kn} \\ &= \sum_{k=i}^n \frac{\prod_{l=i, l \neq k}^n \binom{l}{2}}{\prod_{l=i, l \neq k}^n \left[\binom{l}{2} - \binom{k}{2} \right]} \times \frac{\binom{k}{2}}{\binom{n}{2}} \\ &= \prod_{l=i}^{n-1} \binom{l}{2} \sum_{k=i}^n F_{i,k,n} \\ &= \prod_{l=i}^{n-1} \binom{l}{2} \sum_{k=i}^n (-1) \sum_{l=i, l \neq k}^n F_{i,l,n} \\ &= (-1) \prod_{l=i}^{n-1} \binom{l}{2} \sum_{l=i}^n \sum_{k=i, k \neq l}^n F_{i,l,n} \\ &= (-1)(n-i) \prod_{l=i}^{n-1} \binom{l}{2} \sum_{l=i}^n F_{i,l,n} \\ &= (-1)(n-i) C_{in}. \end{aligned} \quad (14)$$

In the above calculation, we go from line 3 to line 4 by using equation 12. Then on the next line we exchange the two sums and by noticing that the terms under the k -indexed sum are not dependent on k , we obtain line 6. On line 6, we can notice that the factor after $(-1)(n-k)$ is exactly the same as in line 3, thus is equal to C_{in} . Since $n \neq k$, only $C_{in} = 0$ can satisfy $C_{in} = (i-n)C_{in}$.

We go on by computing our second case: the coefficients C_{ij} for $i < j < n$:

$$\begin{aligned} C_{ij} &= \sum_{k=2}^n A_{ik} B_{kj} \\ &= \sum_{k=i}^j A_{ik} B_{kj} \\ &= \sum_{k=i}^j \frac{\prod_{l=i, l \neq k}^n \binom{l}{2}}{\prod_{l=i, l \neq k}^n \left[\binom{l}{2} - \binom{k}{2} \right]} \times \frac{\binom{k}{2}}{\binom{j}{2}} \prod_{l=j+1}^n \left(1 - \frac{\binom{k}{2}}{\binom{l}{2}} \right) \\ &= \prod_{l=i}^{j-1} \binom{l}{2} \sum_{k=i}^j \frac{\prod_{l=j+1}^n \left[\binom{l}{2} - \binom{k}{2} \right]}{\prod_{l=i, l \neq k}^n \left[\binom{l}{2} - \binom{k}{2} \right]} \\ &= \prod_{l=i}^{j-1} \binom{l}{2} \sum_{k=i}^j F_{i,k,j} \\ &= \prod_{l=i}^{j-1} \binom{l}{2} \sum_{k=i}^j (-1) \sum_{l=i, l \neq k}^j F_{i,l,j} \\ &= (-1) \prod_{l=i}^{j-1} \binom{l}{2} \sum_{l=i}^j \sum_{k=i, k \neq l}^j F_{i,l,j} \\ &= (-1)(j-k) \prod_{l=i}^{j-1} \binom{l}{2} \sum_{l=i}^j F_{i,l,j} \\ &= (-1)(j-k) C_{ij}. \end{aligned} \quad (15)$$

Similarly to the computation of C_{in} above, the only way to satisfy $C_{ij} = (i-j)C_{ij}$ for $i < j < n$ is to have $C_{ij} = 0$. Now, the remaining coefficients to be computed are the diagonal coefficients. For

$2 \leq i < n$:

$$\begin{aligned} C_{ii} &= A_{ii} B_{ii} \\ &= \frac{\prod_{l=i+1}^n \binom{l}{2}}{\prod_{l=i+1}^n \left[\binom{l}{2} - \binom{i}{2} \right]} \times \frac{\binom{i}{2}}{\binom{i}{2}} \prod_{l=i+1}^n \left(1 - \frac{\binom{i}{2}}{\binom{l}{2}} \right) \\ &= 1. \end{aligned} \quad (16)$$

Finally,

$$C_{nn} = A_{nn} B_{nn} = 1 \quad (17)$$

All the above computed coefficients prove that the matrix \mathbf{C} is the identity matrix, hence \mathbf{B} is the inverse matrix of \mathbf{A} , which achieves to demonstrate theorem .

Supporting Information

The *ms* commands for the simulations.

All the times are given in units of 2 times the present haploid population size (see tab:s1 to tab:s4 for the exact values). The letter *n* can be replaced by any desired sample size.

- **scenario 1:** `ms n 1 -t 1 -eN 0.025 2 -eN 0.25 0.5 -eN 0.5 1.5 -T`
- **scenario 2:** `ms n 1 -t 1 -G 6.93 -eG 0.2 0.0 -eN 0.3 0.5 -T`
- **scenario 3:** `ms n 1 -t 1 -G -0.732408192445406 -eG 1.5 0.0 -eN 2 4 -eN 3 3`
- **scenario 4:** `ms n 1 -t 1 -G 4605.17018598809 -eG 0.001 -2302.58509299405 -eG 0.002 0 -eN 0.003 0.2 -eN 0.0035 0.05 -eN 0.004 0.1`

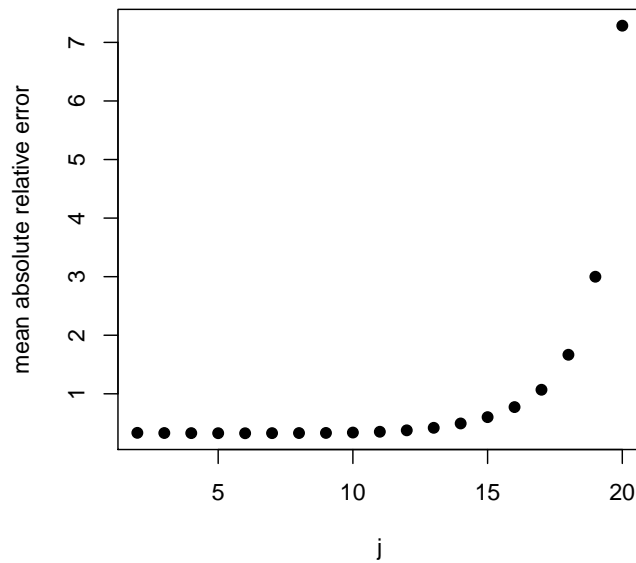


Figure S1 Accuracy of estimates of recent N as function of j . We compare estimates of N under scenario 1 with $n = 20$, between present and generation 1000 back in the past. Time is discretized in 100 equally sized bins and the accuracy of the N estimation is measured by the average relative error (see equation 10 in the main text).

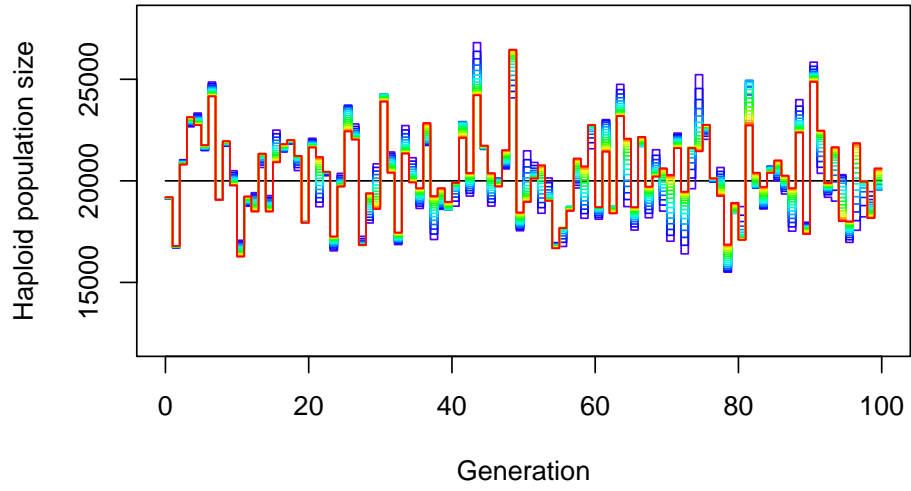


Figure S2 Estimation of $N(t)$ depending on j during the first generations, scenario 1. Different values of j are indicated by the color of the solid lines, with a rainbow gradient from red ($j = 2$) to dark blue ($j = 20$).

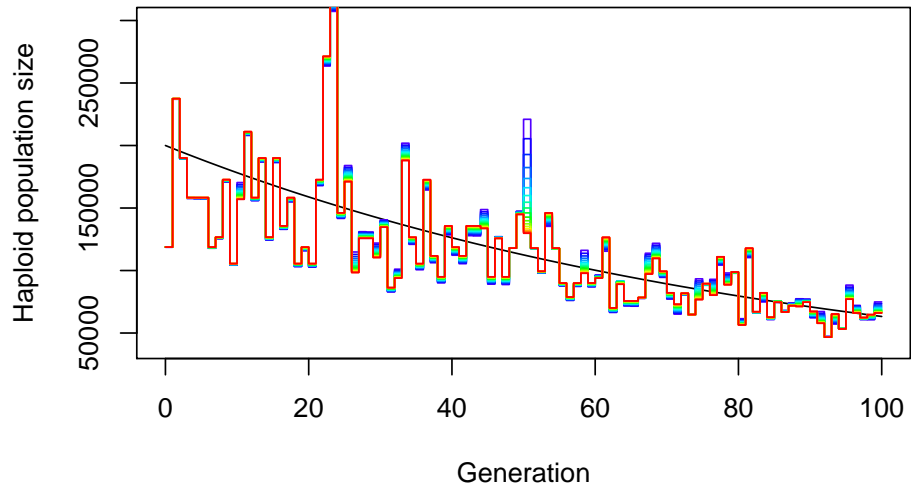


Figure S3 Estimation of $N(t)$ depending on j during the first generations, scenario 4. Different values of j are indicated by the color of the solid lines, with a rainbow gradient from red ($j = 2$) to dark blue ($j = 20$).

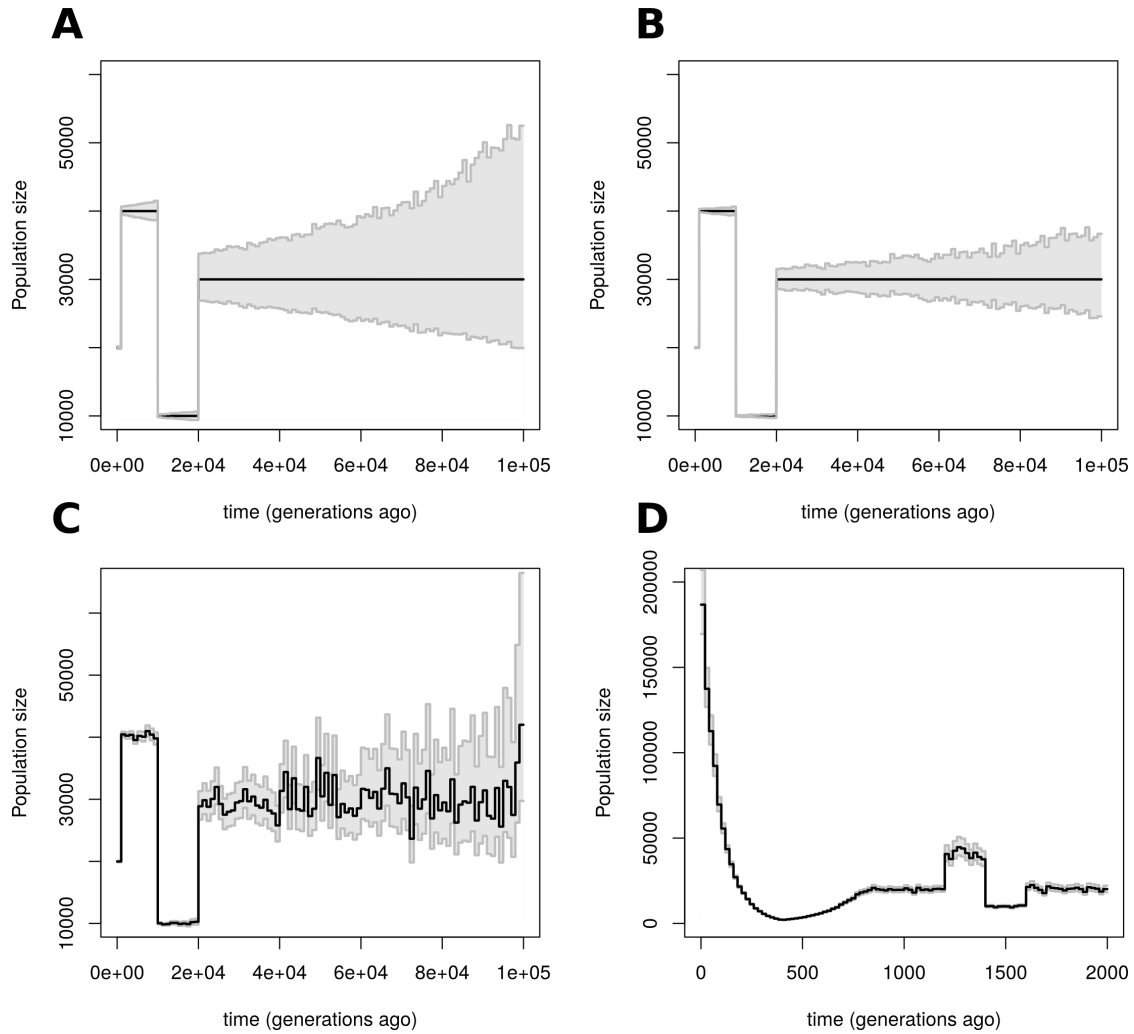


Figure S4 Uncertainty on the estimates of $N(t)$. Results obtained by first simulating 1,000,000 independent gene-genealogies from model 1 with 20 haploid gene-copies and then (A) apply the theorem 10,000 times using 10,000 randomly sampled gene-genealogies from the 1,000,000 genealogies, or (B) apply the theorem 10,000 times using 50,000 randomly sampled gene-genealogies from the 1,000,000 genealogies. (C) Bootstrap results for model 1 using 20,000 gene-genealogies and 10,000 bootstrap replicates. (D) Bootstrap results for model 4 using 20,000 gene-genealogies and 10,000 bootstrap replicates. Time is discretized into 100 equally long intervals. We marked by a two solid gray lines the 2.5 and 97.5 percentiles of the 10,000 estimates of N within each interval. For (A) and (B), the black solid line represents the true value of $N(t)$. For (C) and (D), the black solid line represents the reconstructed $N(t)$ profile using our method on the 20,000 independent gene-genealogies.

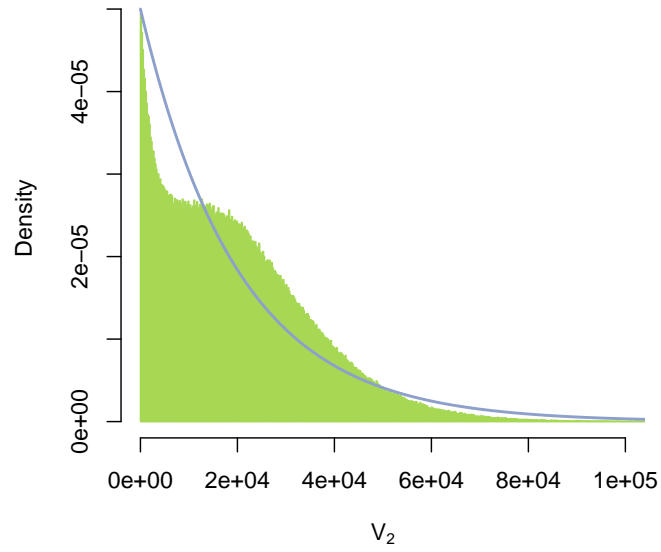


Figure S5 Density of V_2 with cryptic recombination. Comparison between the expected density of V_2 under the constant model for $n = 2$ (solid blue line) and the observed density of V_2 under the constant model with recombination of $Lr = 10^{-4}$ in green.

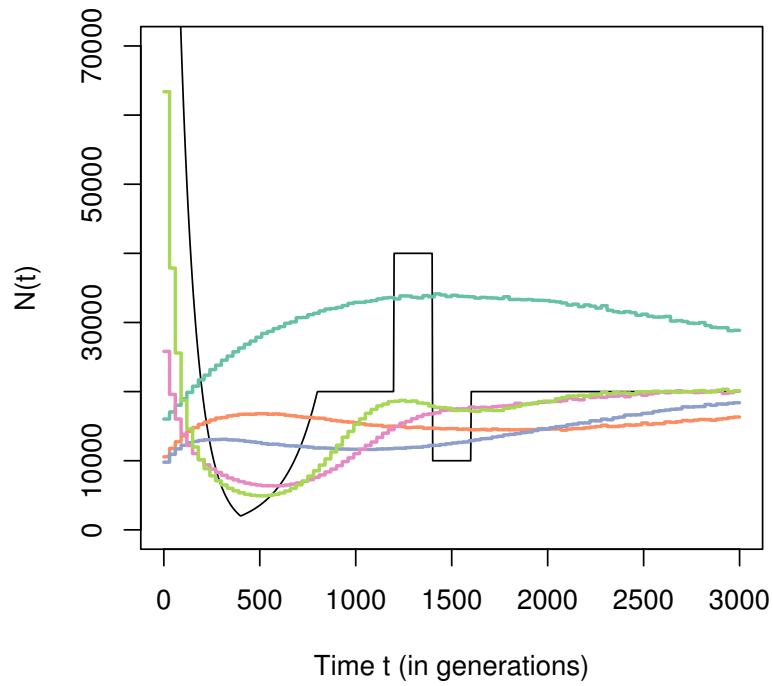
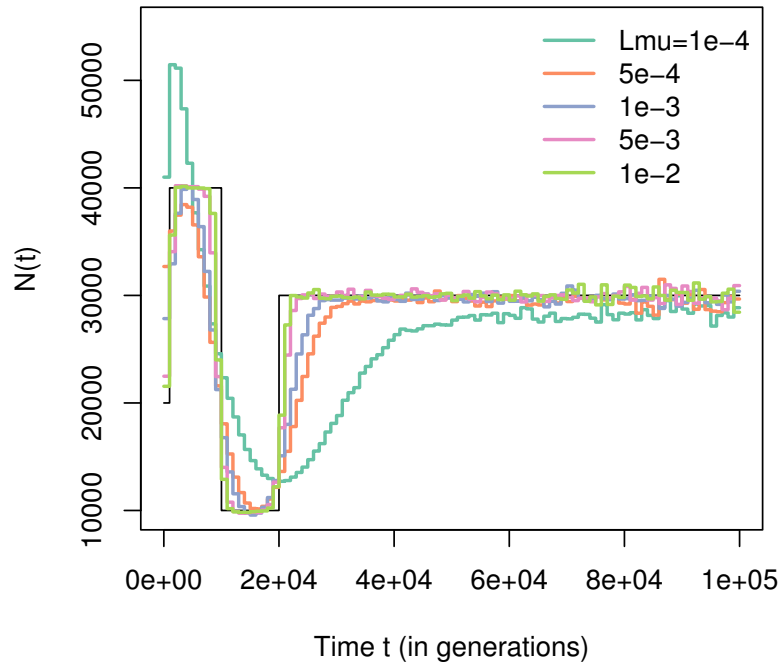


Figure S6 Effect of estimating trees from polymorphism data. Results of the 2 steps reconstruction method, applied with a sample size of 20, for 1,000,000 independent loci, evolving under scenario 1 (top figure) and scenario 4 (bottom figure). The mutation rate per locus $L\mu$ is indicated by the color of the line and the legend gives the correspondence between the colors and the values.

Comparison between methods (CEU)

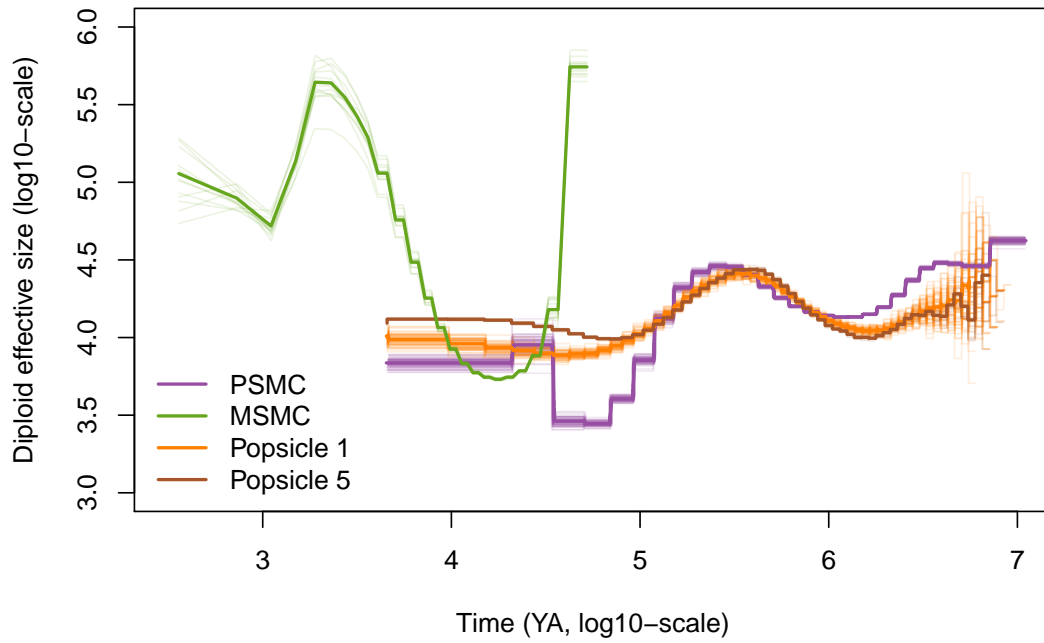


Figure S7 Comparison of methods on the CEU individuals. Log-scale transformed results of the main text figure 7, panel A.

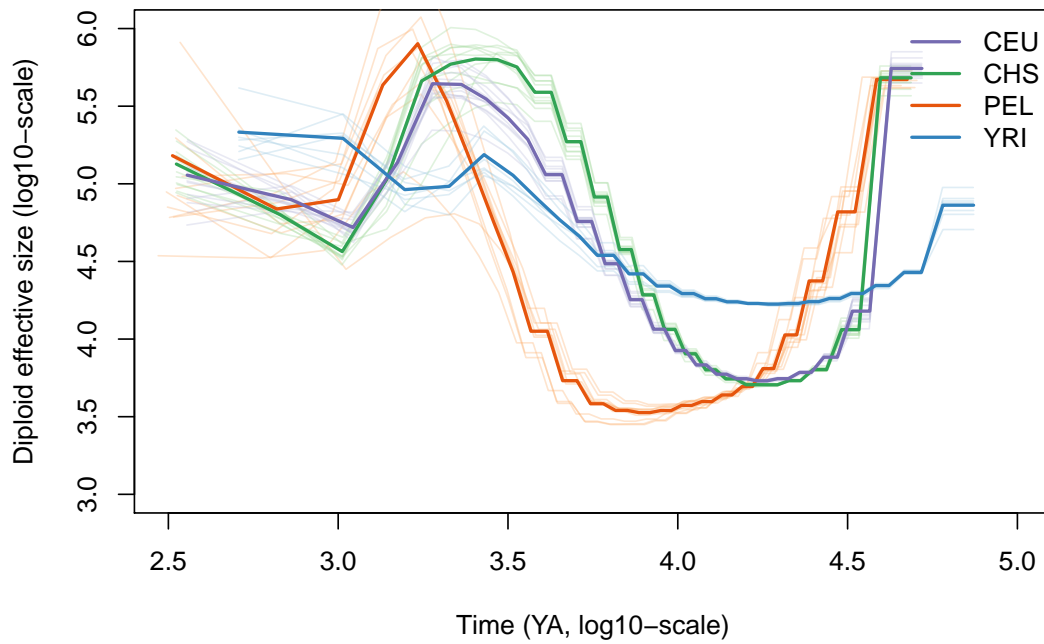


Figure S8 Results of MSMC on CEU, CHS, PEL and YRI. Thin light lines represent the population size reconstruction for one individual and thick lines indicate the average across individuals for a given population. Individuals from PEL have more variance in the estimated scaled mutation rate by MSMC, thus have time intervals that differ quite a bit from individual to individual when scaled back in years.

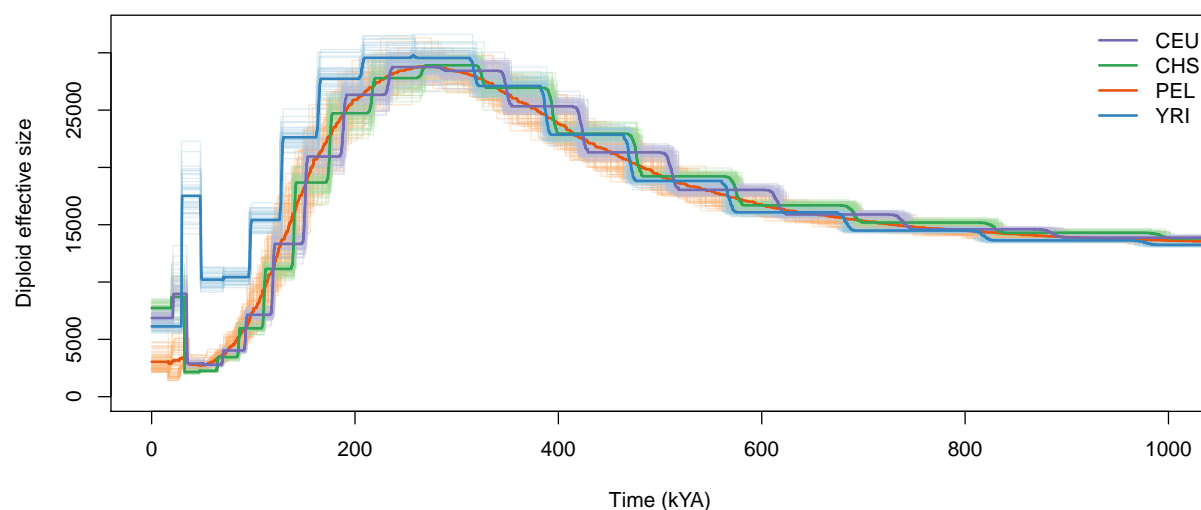


Figure S9 Results of PSMC on CEU, CHS, PEL and YRI. Thin light lines represent the population size reconstruction for one individual and thick lines indicate the average across individuals for a given population. Individuals from PEL have more variance in the estimated scaled mutation rate by PSMC, thus have time intervals that differ quite a bit from individual to individual when scaled back in years.

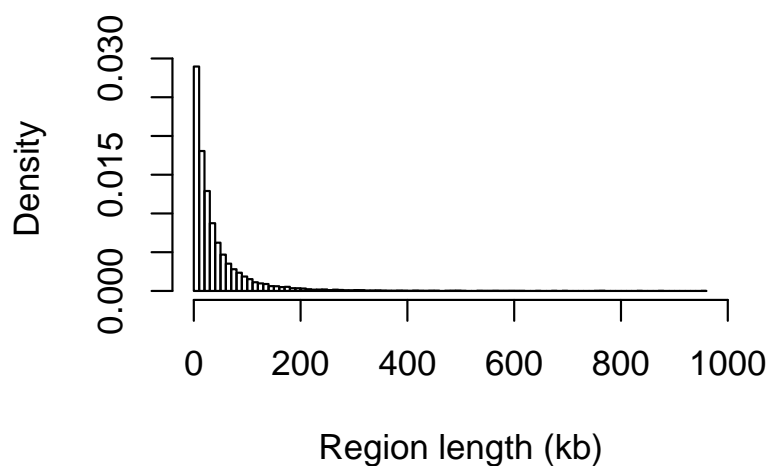


Figure S10 Distribution of length for the no recombining regions of the Decode genetic map.

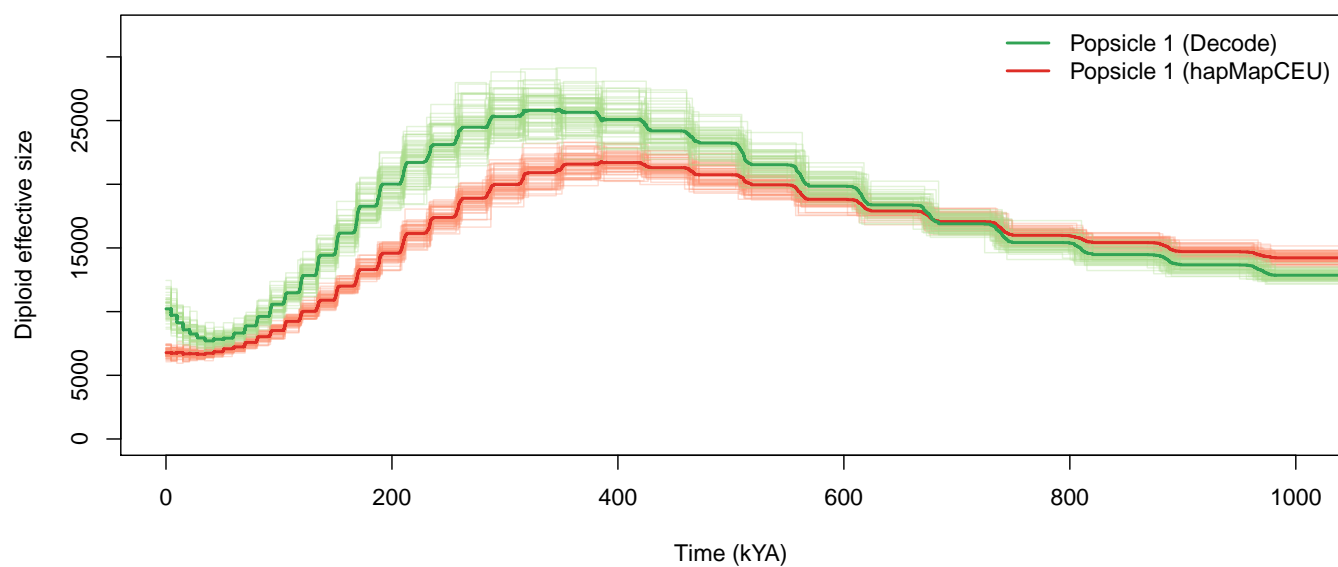


Figure S11 Comparison between Popsicle 1 using no recombining Decode regions (green lines) and Popsicle 1 using low recombining regions extracted from HapMapCEU. CEU samples.

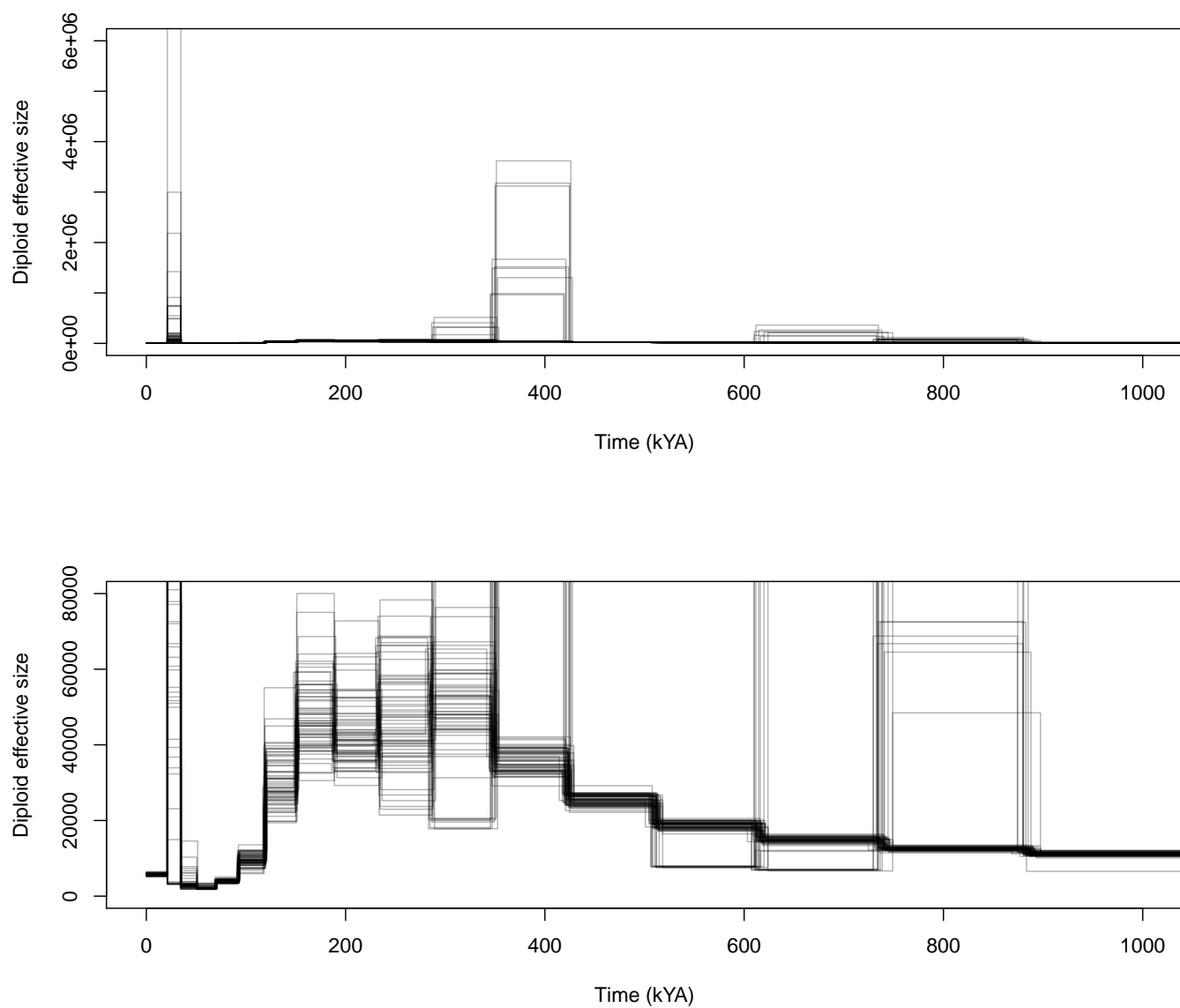


Figure S12 Application of Popsicle 1 to PSMC decoding gene-genealogies. Lower panel is a zoom in of the upper panel curve for smaller population size.

Table S1 Scenario 1

Period (in gen.)	Haploid Size
0-1,000	20,000
1,000-10,000	40,000
10,000-20,000	10,000
> 20,000	30,000

Table S2 Scenario 2

Period (in gen.)	Haploid Size	Parameters
0-16,000	$N_0 \exp(-\alpha t)$	$N_0 = 40,000, \alpha = 6.93/(2N_0)$
16,000-24,000	10,000	
> 24,000	20,000	

Table S3 Scenario 3

Period (in gen.)	Haploid Size	Parameters
0-30,000	$N_0 \exp(-\alpha t)$	$N_0 = 10,000, \alpha = -0.732/(2N_0)$
30,000-40,000	30,000	
40,000-60,000	40,000	
> 60,000	30,000	

Table S4 Scenario 4

Period (in gen.)	Haploid Size	Parameters
0-400	$N_0 \exp(-\alpha_1 t)$	$N_0 = 200,000, \alpha_1 = 4605.2/(2N_0)$
400-800	$N_1 \exp(-\alpha_2(t - 400))$	$N_1 = 2,000, \alpha_2 = -2302.6/(2N_0)$
800-1,200	20,000	
1,200-1,400	40,000	
1,400-1,600	10,000	
> 1,600	20,000	